Article

Benchmarking the Fluxional Processes of Organometallic Piano-Stool Complexes

Nathan C. Frey [ID]**, Eric Van Dornshuld and Charles Edwin Webster ***

Department of Chemistry, Mississippi State University, 310 President's Circle, Starkville, MS 39762-9573, USA; ncf74@msstate.edu (N.C.F.); edornshuld@chemistry.msstate.edu (E.V.D.)
* Correspondence: ewebster@chemistry.msstate.edu

Abstract: The correlation consistent Composite Approach for transition metals (ccCA-TM) and density functional theory (DFT) computations have been applied to investigate the fluxional mechanisms of cyclooctatetraene tricarbonyl chromium ($(COT)Cr(CO)_3$) and 1,3,5,7-tetramethylcyclooctatetraene tricarbonyl chromium, molybdenum, and tungsten ($(TMCOT)M(CO)_3$ (M = Cr, Mo, and W)) complexes. The geometries of $(COT)Cr(CO)_3$ were fully characterized with the PBEPBE, PBE0, B3LYP, and B97-1 functionals with various basis set/ECP combinations, while all investigated $(TMCOT)M(CO)_3$ complexes were fully characterized with the PBEPBE, PBE0, and B3LYP methods. The energetics of the fluxional dynamics of $(COT)Cr(CO)_3$ were examined using the correlation consistent Composite Approach for transition metals (ccCA-TM) to provide reliable energy benchmarks for corresponding DFT results. The PBE0/BS1 results are in semiquantitative agreement with the ccCA-TM results. Various transition states were identified for the fluxional processes of $(COT)Cr(CO)_3$. The PBEPBE/BS1 energetics indicate that the 1,2-shift is the lowest energy fluxional process, while the B3LYP/BS1 energetics (where BS1 = H, C, O: 6-31G(d'); M: mod-LANL2DZ(f)-ECP) indicate the 1,3-shift having a lower electronic energy of activation than the 1,2-shift by 2.9 kcal mol^{-1}. Notably, PBE0/BS1 describes the $(CO)_3$ rotation to be the lowest energy process, followed by the 1,3-shift. Six transition states have been identified in the fluxional processes of each of the $(TMCOT)M(CO)_3$ complexes (except for $(TMCOT)W(CO)_3$), two of which are 1,2-shift transition states. The lowest-energy fluxional process of each $(TMCOT)M(CO)_3$ complex (computed with the PBE0 functional) has a $\Delta G^{\ddagger}$ of 12.6, 12.8, and 13.2 kcal mol^{-1} for Cr, Mo, and W complexes, respectively. Good agreement was observed between the experimental and computed ^{1}H-NMR and ^{13}C-NMR chemical shifts for $(TMCOT)Cr(CO)_3$ and $(TMCOT)Mo(CO)_3$ at three different temperature regimes, with coalescence of chemically equivalent groups at higher temperatures.

Keywords: fluxionality; piano-stool complexes; variable-temperature NMR; DFT; ccCA-TM; computational benchmarking and calibration

1. Introduction

Fluxional molecules are dynamic compounds in which magnetically or chemically distinct groups can readily interchange positions. The stereochemically fluid nature of such molecules at room temperature is illustrated by the fluxional shifts that they undergo [1–3]. These systems perform a significant role in increasing enantioselectivity in asymmetric synthesis [4–10]. CpRu((R)-BINOP-F)(H$_2$O)][SbF$_6$] has been used as a catalyst in the Diels–Alder reaction of methacrolein and cyclopentadiene to produce a [4+2] cycloadduct with enantioselectivity of 92% ee (exo) [9]. During this reaction, the catalyst was shown to exhibit a fluxional pendular motion of the BINOP-F ligand, thereby creating chemically equivalent environments about the two phosphorus substituents.

Density functional theory (DFT) is a useful tool used to characterize the details in the fluxional behavior of various complexes [11]. Previous studies incorporating DFT on fluxional systems range from biochemical applications, such as Cu (II)···GlyHisLys peptide

binding [12] to understanding fluxionally chiral dimethylaminopyridine catalysts [4,10]. Haptotropic rearrangement processes in sandwich-type complexes have also been investigated by DFT approaches [13–15]. Similarly, DFT has been used to gain insight into the fluxionality of various ligands, such as phosphines, in transition metal complexes by way of simulated NMR spectroscopy [16,17].

Although DFT has been used to characterize the energetics of fluxional processes, composite approaches have yet to be utilized to calibrate DFT results on these systems. The correlation consistent Composite Approach for transition metals (ccCA-TM) has been previously utilized to benchmark energetics of transition metal complexes [18–25], and it has been shown to have a mean absolute deviation (MAD) from experiment of 3.0 kcal mol^{-1} ("transition-metal chemical accuracy"). The ccCA-TM methodology was utilized in this study of cyclooctatetraene chromium tricarbonyl ((COT)Cr(CO)$_3$) to provide reliable energies for which to compare DFT results.

Cyclooctatetraene tricarbonyl d^4 complexes ((COT)M(CO)$_3$) are fluxional molecules that contain an η^6-bound COT ligand that results in a "piano-stool" conformation (Figure 1A) [26]. In order to be comprehensive and specific, we provide, in Figure 1, an explicit accounting of the possible shifts in COT-type complexes. The lowest energy geometry for the (COT)M(CO)$_3$ molecule is a piano-stool structure (**A** in Figure 1). These complexes can undergo a variety of fluxional shifts in which metal–COT carbon interactions are disrupted and then bound on a new carbon of the COT ligand. These processes can be denoted as a 1,*n*-shift (*n* = 2, 3, 4, 5), where *n* represents the carbon on the ring to which the reference bond on the ring has moved. For example, a 1,2-shift indicates a bonding rearrangement from the parent configuration ([1–6]-η^6 geometry, **i** in Figure 1) to another η^6 configuration ([2–7]-η^6 geometry, **ii** in Figure 1). Therefore, a 1,3-shift would result in the parent [1–6]-η^6 geometry rearranging to the [3–8]-η^6 geometry (**iii** in Figure 1).
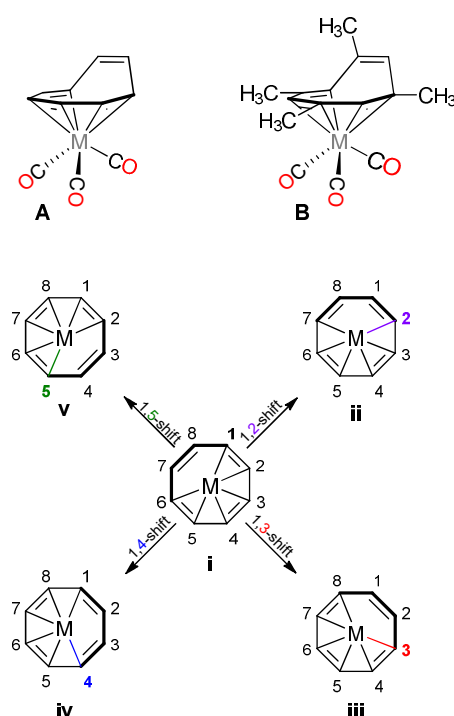

Figure 1. Two-dimensional representations of generalized COT (**A**) and TMCOT (**B**) piano-stool complexes. 1,*n*-shift (*n* = 2, 3, 4, 5) in (COT)M(CO)$_3$/(TMCOT)M(CO)$_3$. CO, H, and CH$_3$ groups omitted for clarity (**i**–**v**).

Historical studies demonstrate that variable temperature NMR (VT-NMR) is a pivotal tool in understanding fluxional behavior [27]. For example, VT ^{1}H-NMR spectra provide insight into the energetics of the valency tautomerism of COT ligands about the metal

center of (COT)M(CO)$_3$ (M = Cr, Mo) ($\Delta G^{\ddagger}$ = 15.4 kcal mol^{-1} ($k \approx 25$ s^{-1}) at 20 °C for (COT)Cr(CO)$_3$ and $\Delta G^{\ddagger}$ = 14.8 kcal mol^{-1} ($k \approx 25$ s^{-1}) at 10 °C for (COT)Mo(CO)$_3$ [28]. The pioneering work of Cotton and coworkers proposed mechanisms for these low energy rearrangement processes [1,26–30]. Whitesides and Budnik successfully studied the Mo derivative ten years later to arrive at similar conclusions [31]. Spin-saturation [32] and 2D-EXSY [33] have been used to understand fluxional processes. In addition, Lawless and Marynick's study provided insights from semiempirical computations into the ring rearrangement processes for (COT)Cr(CO)$_3$ [34]. In this study, we apply the robust ccCA-TM approach alongside DFT to provide insight into the ring-rearrangement processes of (COT)Cr(CO)$_3$. Various ring-rearrangement pathways, including 1,2-, 1,3-, 1,4-, and 1,5-shifts, and (CO)$_3$ rotation about the metal center, will be considered in the fluxional processes of these complexes. Herein, we report a study of the energetics of (COT)Cr(CO)$_3$ and (TMCOT)M(CO)$_3$ (M = Cr, Mo, W), and an analysis of VT-NMR spectra for (TMCOT)Cr(CO)$_3$ and (TMCOT)Mo(CO)$_3$.

2. Results

Figure 2 is the potential energy surface for the ring rearrangement processes of (COT)Cr(CO)$_3$ at various levels of theory, in which one minimum energy structure (**I**) and five transition states (**TS-1** to **TS-5**) were identified. $\Delta E_e^{\ddagger}$ values for the following transition states are given at the PBEPBE/BS1, B3LYP/BS1, and PBE0/BS1 levels of theory (see Methodology for basis set definitions). Additionally, given are the $\Delta E_e^{\ddagger}$ values derived using ccCA-TM. **TS-1** is C_s-symmetric, where the COT ligand is η^6-bound to Cr. This transition state represents the 120° rotation of the three carbonyl groups about the metal center. **TS-2** (1,3-shift) is a C_s-symmetric complex where the COT ligand is η^4-bound to Cr. **TS-3** (1,2-shift) is C_s-symmetric structure such that the COT ligand is η^5-bound to Cr. **TS-4** (1,5-shift) is a C_s-symmetric complex, which possesses an η^4-bound COT ligand. The highest-energy fluxional transition state, **TS-5** (1,4-shift), is a C_s-symmetric complex, where the COT ligand is η^4-bound to Cr. Good agreement was observed in the relative $\Delta E_e^{\ddagger}$ values computed using PBE0/BS1 and those derived using ccCA-TM. Tabulated bond lengths, $\Delta G^{\ddagger}$, $\Delta E_e^{\ddagger}$, and $\Delta\Delta E_e^{\ddagger}$ (relative to ccCA-TM) values computed at each level of theory are given in the Supporting Information (Table S1, Table S2, Table S3, and Table S4, respectively). Method and basis set testing was performed for each (**I**, **TS-1**–**TS-5**).

Additionally, identified were two additional geometries, structure **2** and **TS-6** (see Figure S4). Structure **2** is a local minimum (ΔE_e = 24.3 kcal mol^{-1} using the PBE0/BS1 level of theory) connected to **I** by way of **TS-6** ($\Delta E_e^{\ddagger}$ = 25.3 kcal mol^{-1}). Because **2** is higher in energy than **I**, it was not considered in the fluxional processes of (COT)Cr(CO)$_3$.

The TMCOT ligand in the X-ray crystal structure of (TMCOT)Cr(CO)$_3$ reported by Cotton and coworkers is η^6-bound to Cr. An overlay of experimental and PBE0/BS1 optimized structures is shown in Figure 3.

The XRD structure (CSD entry: TMCOCR) [29] matches well with the optimized geometry of the lowest energy structure (**II**) for (TMCOT)Cr(CO)$_3$ (RMSD = 0.038 Å for the 19 heavy atoms using PBE0/BS1 optimized structure). The X-ray crystal structures for the Mo and W complexes have not been reported. However, the computed structures for these derivatives each contain a η^6-bound TMCOT ligand and appear to be very similar to the lowest-energy structure computed for the Cr complex (RMSD = 0.146 Å for Mo, 1.181 Å for W relative to (TMCOT)Cr(CO)$_3$ for 19 heavy atoms; RMSD calculated using PBE0/BS1 optimized structures).
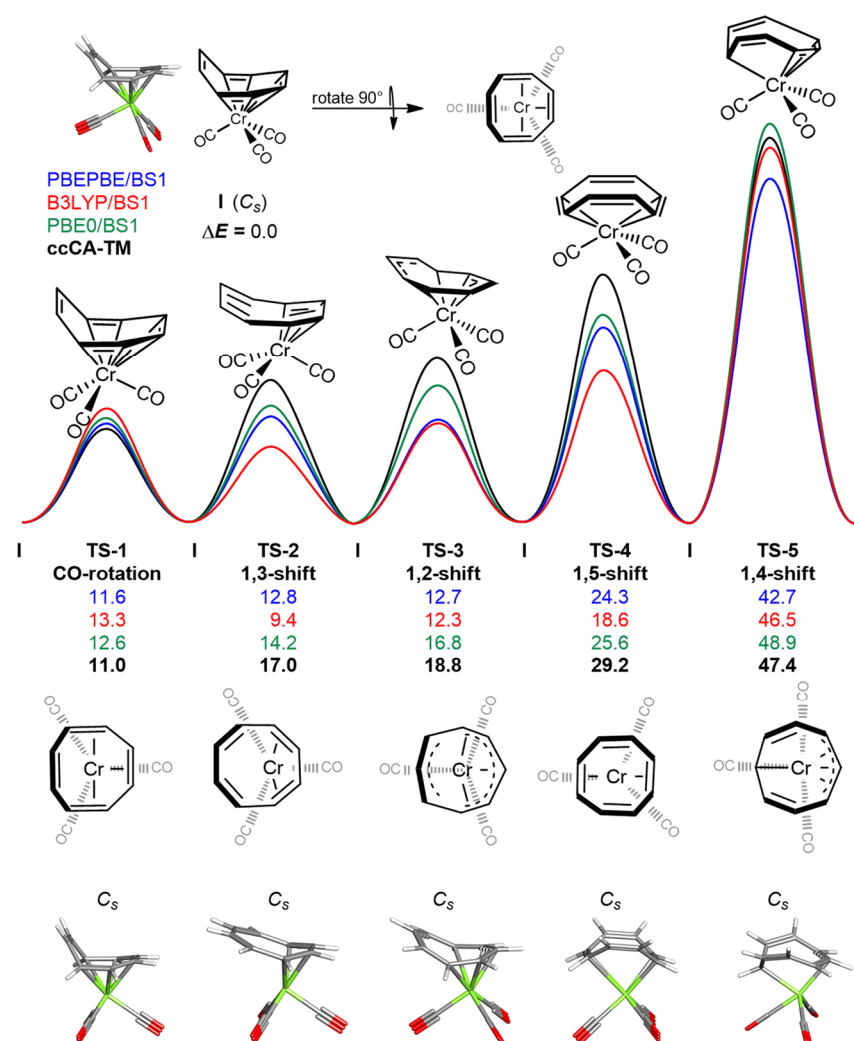
Figure 2. Potential energy surface for the ring rearrangement processes of (COT)Cr(CO)$_3$ at various levels of theory. Relative electronic energies ($\Delta E_e^{\ddagger}$) are given in kcal mol^{-1}. Transition states are ordered in reference to $\Delta E_e^{\ddagger}$ values derived from ccCA-TM.
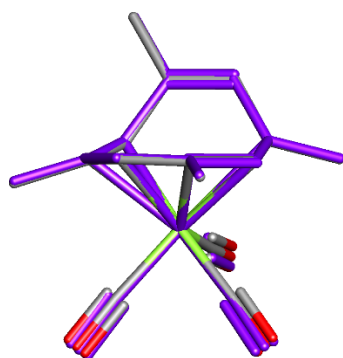

Figure 3. Overlay of the geometry from the X-ray crystal structure (purple) with the PBE0/BS1 optimized structure of (TMCOT)Cr(CO)$_3$. Cr: green, O: red, C: grey (H omitted for clarity).

The potential energy surface for the various rearrangements processes for (TMCOT)Cr(CO)$_3$ is given in Figure 4. The lowest-energy geometry is represented by structure **II**. $\Delta E_e^{\ddagger}$ values for the described transition states are given at the: PBEPBE/BS1, B3LYP/BS1, and PBE0/BS1 levels of theory for (TMCOT)Cr(CO)$_3$. **TS-A** (CO-rotation) is C_1-symmetric and represents a 120° (CO)$_3$ rotation about Cr, where the TMCOT ligand remains η^6-bound to the Cr. The

lowest energy fluxional transition state, **TS-B** (1,2-shift-a), is a C_s-symmetric structure in which TMCOT is η^5-bound to Cr. In **TS-B**, the mirror plane passes through two of the opposing C-H units in the TMCOT ligand. **TS-C** (1,3-shift) is C_1-symmetric, in which the TMCOT ligand is η^4-bound to the Cr atom. **TS-D** (1,5-shift) is a C_1-symmetric structure in which TMCOT is η^4-bound to the metal. **TS-E** (1,2-shift-b) is a C_s symmetric structure in which TMCOT is η^5-bound to the Cr center and represents a second 1,2-shift. The mirror plane in this structure passes through the opposing C–CH$_3$ units, in contrast to the opposing C–H units as seen in **TS-A**. **TS-F** (1,4-shift) represents the transition state in which the complex is C_1-symmetric with an η^4-bound TMCOT ligand.
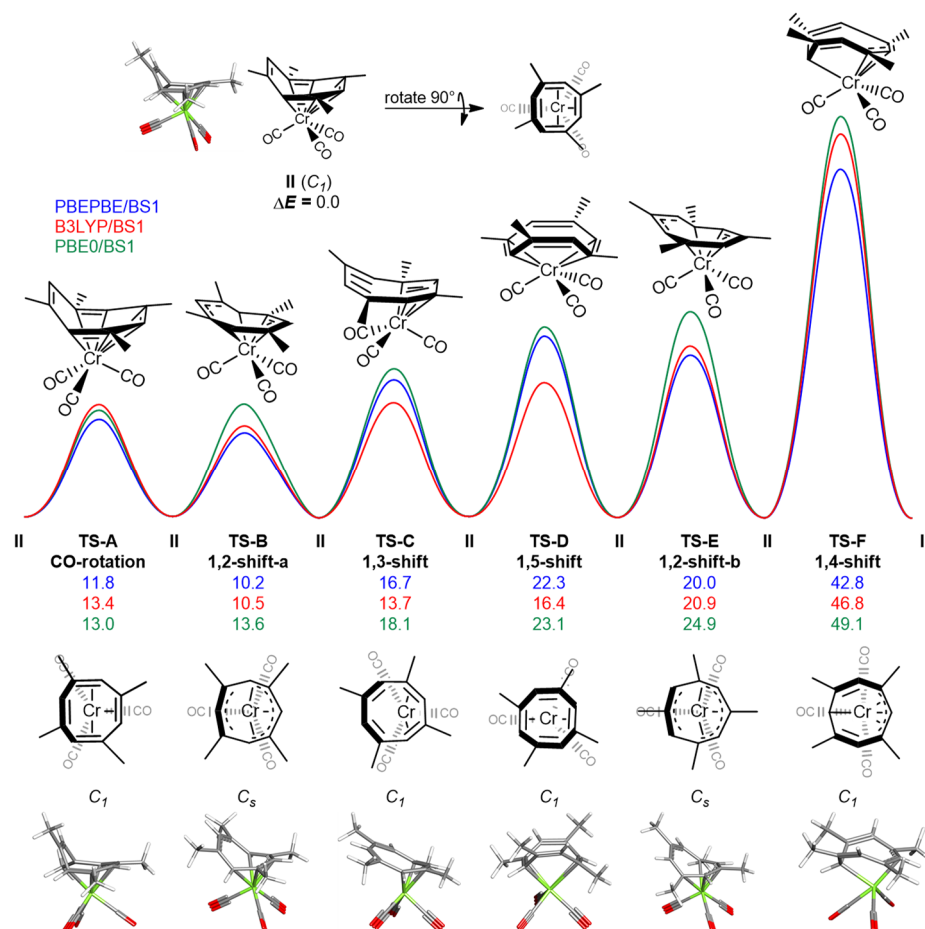

Figure 4. Potential energy surface for various rearrangements in (TMCOT)Cr(CO)$_3$. Relative electronic energies are given in kcal mol^{-1}. Transition states are ordered in reference to $\Delta E_e{}^\ddagger$ values computed using PBE0/BS1.

Table 1 lists the computed relative electronic energies and Gibbs free energies for the different transition states of the (TMCOT)M(CO)$_3$ complexes computed with the PBEPBE, B3LYP, and PBE0 methods using BS1. Notably, PBE0/BS1 computed energies show that **TS-D** for (TMCOT)W(CO)$_3$ is 2.5 kcal mol^{-1} higher in energy than **TS-E**, deviating in the relative $\Delta E_e{}^\ddagger$ ordering depicted in (TMCOT)Cr(CO)$_3$ and (TMCOT)Mo(CO)$_3$. Additionally, there are insignificant differences in the relative energetic ordering of the fluxional processes of each (TMCOT)M(CO)$_3$ complex, depending on the level of theory implemented. The computed relative electronic energies for (TMCOT)M(CO)$_3$ and (COT)Cr(CO)$_3$ can be found in Table 1 and Table S3, respectively. An additional 1,4-shift transition state (**TS-G**) was located computationally for (TMCOT)W(CO)$_3$ (Figure S3).

Table 1. Computed relative electronic energies and free energies (in parentheses) for (TMCOT)M(CO)$_3$ (M = Cr, Mo, W) fluxional transition states with DFT/BS1 (all energies reported in kcal mol^{-1}).

		TS-A (CO-rot)	TS-B (1,2-a)	TS-C (1,3)	TS-D (1,5)	TS-E (1,2-b)	TS-F (1,4)
M = Cr							
	PBEPBE	11.8 (12.0)	10.2 (9.7)	16.7 (16.6)	22.3 (20.6)	20.0 (17.3)	42.8 (41.8)
	B3LYP	13.4 (13.8)	10.5 (9.9)	13.7 (13.9)	16.4 (15.0)	20.9 (18.1)	46.8 (44.8)
	PBE0	13.0 (13.4)	13.6 (12.6)	18.1 (18.0)	23.1 (21.3)	24.9 (21.9)	49.1 (47.9)
M = Mo							
	PBEPBE	12.0 (12.7)	10.1 (9.7)	15.3 (15.9)	19.0 (18.4)	19.9 (18.3)	41.4 (40.8)
	B3LYP	14.0 (14.5)	10.6 (9.9)	13.7 (14.3)	15.5 (15.0)	21.2 (18.8)	44.5 (43.7)
	PBE0	13.3 (13.8)	13.6 (12.8)	17.5 (18.0)	21.1 (20.3)	24.7 (22.5)	47.0 (46.3)
M = W							
	PBEPBE	10.2 (10.8)	10.7 (10.1)	19.3 (19.7)	24.7 (23.2)	21.2 (19.7)	40.9 (40.1)
	B3LYP	11.6 (12.3)	10.4 (9.9)	17.2 (17.8)	21.7 (21.0)	21.5 (19.8)	42.2 (41.6)
	PBE0	11.1 (11.6)	14.0 (13.2)	22.1 (22.3)	28.2 (26.9)	25.7 (23.8)	45.8 (45.1)

3. Discussion

Several DFT methods utilized for the (COT)Cr(CO)$_3$ system disagreed with the relative energy ordering of the fluxional processes obtained with the more rigorous ccCA-TM methodology. It is helpful to determine which methodology is in closest agreement with this composite approach. After testing several levels of theory, it was found that PBE0/BS1 and PBE0/BS3 computed $\Delta E_e{}^{\ddagger}$ values do indeed qualitatively correlate with ccCA-TM. Consequently, PBE0/BS1 was extended to the larger, less symmetric (TMCOT)M(CO)$_3$ systems. Notably, ccCA-TM relative energetics computed using the weighted and non-weighted double-ζ basis sets for CCSD(T) and CCSD(T, FC1) single points were isoenergetic within 0.1 kcal mol^{-1}.

The $\Delta E_e{}^{\ddagger}$ values for (COT)Cr(CO)$_3$ computed using the PBE0/BS1 and PBE0/BS3 levels of theory were both in agreement with the relative ordering presented by ccCA-TM. However, PBEPBE energetics computed with BS1, BS2, and BS3 each showed that the 1,2 and 1,3-shifts were nearly isoenergetic with an energy difference of 0.2 kcal mol^{-1}. B3LYP electronic energetics computed with BS1, BS3, and BS5 each showed that the 1,3-shift was the lowest energy structure, where the 1,2-shift was lower in energy than the CO-rotation. The electronic energies computed at the B97-1/BS2 and B97-1/BS3 levels of theory depicted that the 1,3-shift was the lowest energy process, followed by the CO-rotation and the 1,2-shift. This data is provided in Table S3.

It is evident that for (COT)Cr(CO)$_3$, the 1,3-shift is indeed the lowest energy fluxional process based on experimental and computational results. The experimental $\Delta G^{\ddagger}$ value for the 1,3-shift of (COT)Cr(CO)$_3$ was reported to be 15.2 kcal mol^{-1}, which is 1.7 kcal mol^{-1} higher than the PBE0/BS1 computed $\Delta G^{\ddagger}$ ($\Delta G^{\ddagger}{}_{comp}$) for **TS-2** (13.5 kcal mol^{-1}). There are structural similarities in the transition states of the fluxional processes of each (TMCOT)M(CO)$_3$ complex. Cotton and coworkers found that 1,2-shift-a (**TS-B**) is the first process that causes coalescence in (TMCOT)Cr(CO)$_3$ with a $\Delta G^{\ddagger}$ of 16.0 kcal mol^{-1} ($\Delta G^{\ddagger}{}_{comp}$ = 12.6 kcal mol^{-1} using PBE0/BS1). The experimental activation energy for **TS-B** for the Mo derivative is 16.0 kcal mol^{-1} ($\Delta G^{\ddagger}{}_{comp}$ = 12.8 kcal mol^{-1} using PBE0/BS1, see Table 1), while the experimental activation energy for the W complex is 19.3 kcal mol^{-1} [30] ($\Delta G^{\ddagger}{}_{comp}$ = 13.2 kcal mol^{-1} using PBE0/BS1, see Table 1).

Solvation of (TMCOT)M(CO)$_3$ in chloroform SMD raises the $\Delta G^{\ddagger}$ of most transition states, and slightly alters the relative ordering of the fluxional processes of each (TMCOT)M(CO)$_3$ complex (Table S7).

Simulated ^{1}H-NMR and ^{13}C-NMR spectra computed at the GIAO-PBE0/BS6//PBE0/BS1 level of theory (Figures 5 and 6, respectively) show that coalescence of peaks is observed when higher temperature regimes are considered. When the temperature is increased, higher energy fluxional transition states are more easily accessible for (COT)Cr(CO)$_3$ and (TMCOT)M(CO)$_3$.
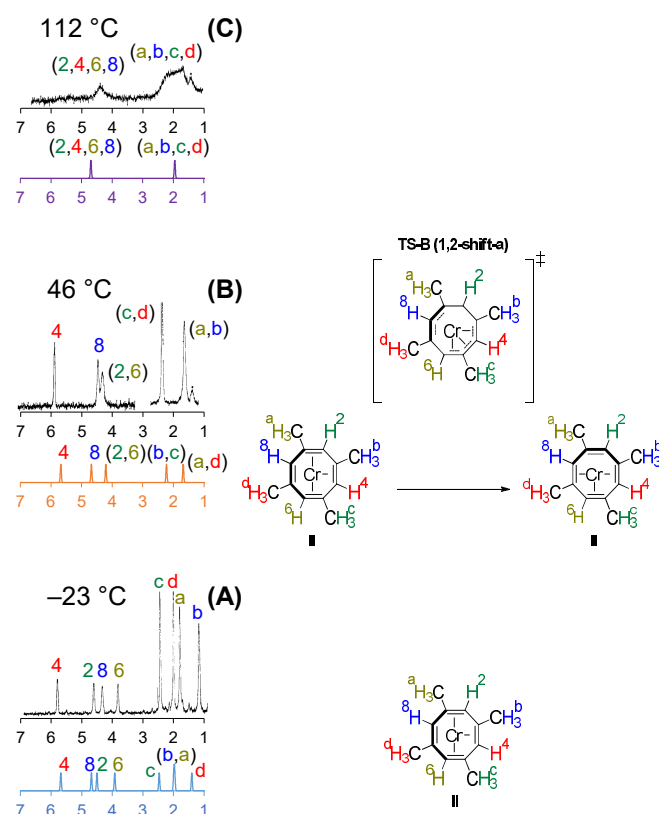
Figure 5. Simulated gas-phase (colored, GIAO-PBE0/BS6//PBE0/BS1) and experimental ^{1}H-NMR for (TMCOT)Cr(CO)$_3$ in three temperature regimes (**A**–**C**) with corresponding fluxional processes. (CO)$_3$ omitted for clarity. All chemical shifts are relative to tetramethylsilane (TMS). The experimental ^{1}H-NMR spectra (black) have been adapted in part with permission from Cotton, F. A.; Faller, J. W.; Musco, A., Stereochemically nonrigid organometallic molecules. XII. Temperature dependence of the proton nuclear magnetic resonance spectra of the 1,3,5,7-tetramethylcyclooctatetraene tricarbonyl compounds of chromium, molybdenum, and tungsten *J. Am. Chem. Soc.*, **1968**, *90* (6), 1438-1444. Copyright (1968) American Chemical Society [30].

The experimental and computed ^{1}H-NMR spectra of (TMCOT)Cr(CO)$_3$ illustrate that there are eight distinct peaks at −23 °C (Figure 5A). In the computed gas-phase ^{1}H-NMR spectrum, the peaks for vinyl protons **8** and **2** have reversed assignments when compared to experimental results. Cotton and coworkers stated that there was no basis for assigning the peaks for the methyl groups in the low-temperature limit ^{1}H-NMR spectrum, so the experimental labeling is arbitrary [30]. The computed assignments for the methyl peaks are **b**, **c**, **a**, **d** (downfield to upfield) while the experimental assignments were **c**, **d**, **a**, **b** (downfield to upfield) (Figure 5A).

Increasing the temperature to 46 °C leads to coalescence of equivalent vinyl protons **2**/**6** and the methyl protons represented by **b**/**c** and **a**/**d**, respectively, while vinyl protons **4** and **8** remain chemically distinct. This leads to five discernable peaks: three for the vinyl protons and two for the methyl protons (Figure 5B).

At 112 °C, the vinyl protons coalesce near 5 ppm while the methyl protons coalesced around 2 ppm (Figure 5C). Simulated gas-phase ^{1}H-NMR spectra for (TMCOT)Mo(CO)$_3$ resembles that of (TMCOT)Cr(CO)$_3$ in each of the three temperature regimes (Figure S5).

The experimental VT ^{13}C-NMR spectrum of (TMCOT)Cr(CO)$_3$ shows twelve distinct peaks (^{13}C-NMR chemical shifts for CO groups were not reported) [26] at low temperature while the simulated spectrum shows fifteen distinct peaks (Figure 6A). By increasing the temperature to an intermediate temperature, the peaks for carbons **4** and **8** of the TMCOT ligand remain chemically non-equivalent (Figure 6B). However, coalescence of peaks is observed in carbons **1**/**7**, **3**/**5**, **2**/**6**, **b**/**c**, and **a**/**d**, and carbons **9**/**10**/**11** (only observed

computationally), thereby indicating a 1,2-shift within this temperature region. Due to the rotation rate of the three CO ligands about the Cr atom, all CO ligands are chemically equivalent. At high temperatures, coalescence is observed in each the olefin carbons, methyl carbons, and carbonyl carbons, respectively (Figure 6C).
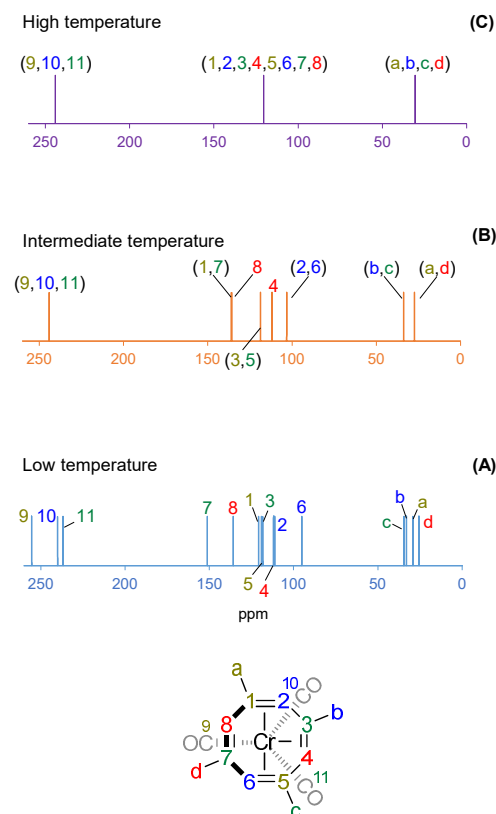

Figure 6. Simulated GIAO-PBE0/BS6//PBE0/BS1 ^{13}C-NMR spectrum of (TMCOT)Cr(CO)$_3$ at low temperature (**A**), intermediate temperature (**B**), and high temperature (**C**). Chemical shifts are relative to TMS.

4. Materials and Methods

All computations were performed using Gaussian 09 Revision D.01 [35]. All DFT computations were performed with a pruned fine integration grid with 75 radial shells and 302 angular points per shell. For all (COT)Cr(CO)$_3$ complexes, full geometry optimizations and corresponding harmonic vibrational frequency computations were performed using the PBEPBE/BS1 [36–38], PBE0/BS1 [39], PBEPBE/BS2, B3LYP/BS1 [40,41], B3LYP/BS3, B3LYP/BS4, B3LYP/BS5, B97-1/BS2 [42,43], and B97-1/BS3 levels of theory (BS1 = 6-31G(d′) for H, C, O; mod-LANL2DZ(f)) [44–46] with effective core potential (ECP) for transition metals, LANL2DZ(d,p) [47,48] with ECP for Si, BS2 = 6-311++G(2df,2p) [49,50] for H, C, O; mod-LANL2TZ [45,48,51] uncontracted to [4s4p3d] for Cr, BS3 = cc-pVTZ [52–55] for all atoms, BS4 = aug-cc-pVDZ [56] for H, C, O; LANL2DZ with LANL2DZ ECP for Cr, BS5 = aug-cc-pVDZ for H, C, O; SDD [57,58] with SDD ECP for Cr). All PBEPBE/BS1 computations were performed using the density fitting procedure as implemented in Gaussian 09 [59–62].

Single point computations were performed at the HF/aug-cc-pVXZ-DK (X = D, T, Q) [56,63,64], MP2/aug-cc-pVXZ-DK (X = D, T, Q) [56,63,65–70], MP2/cc-pVTZ-DK [63,71], CCSD(T)/cc-pVXZ-DK (X = D, T) [63,72–76], CCSD(T)/aug-cc-pwCVDZ-DK [54], CCSD(T, FC1)/aug-cc-pVDZ-DK, and CCSD(T, FC1)/aug-cc-pwCVDZ-DK levels of theory on B3LYP/BS3 optimized geometries with Douglas–Kroll–Hess 2nd order scalar relativistic calculations [77–82] in order to derive the correlation consistent Composite Approach for tran-

sition metals (ccCA-TM) [18–25] energetics for each reported structure of $(COT)Cr(CO)_3$. The total electronic energy described by ccCA-TM is represented by Equation (1).

$$E_{total} = E_{ref}(ccCA) + \Delta E(CC) + \Delta E(CV) + \Delta E(ZPE) + \Delta E(SO) \tag{1}$$

$E_{ref}(ccCA)$ represents energies at the MP2/aug-cc-pVXZ (X = D, T, Q) complete basis set (CBS) limit added to the HF/CBS energy. The HF CBS limit can be computed with a two-point extrapolation of HF energies with the aug-cc-pVTZ and aug-cc-pVQZ basis sets as seen in Equation (2).

$$E(n) = E(CBS) + Ae^{1.63n} \tag{2}$$

Equation (2) can be represented algebraically by Equation (3) [83], where B = 1.63.

$$E_\infty = E_X - \left(\frac{E_X - E_{X+1}}{(1 - e^{-B})} \right) \tag{3}$$

$\Delta E(CC)$ is a correction that stems from CCSD(T) to account for higher order dynamic correlation effects, as it is not adequately described using MP2. $\Delta E(CV)$ represents a basis set correction to the core–core and core–valence electron interactions in CCSD(T). $\Delta E(ZPE)$ is the result of zero-point energy and thermal corrections at 298.15 K, which uses harmonic vibrational frequencies scaled by 0.989. $\Delta E(SO)$ is the atomic spin-orbit coupling correction [84].

For all $(TMCOT)M(CO)_3$ complexes, full geometry optimizations and corresponding harmonic vibrational frequency computations were performed at the PBEPBE/BS1, B3LYP/BS1, and PBE0/BS1 levels of theory.

Magnetic shielding tensors for $(TMCOT)Cr(CO)_3$ and $(TMCOT)Mo(CO)_3$ were computed using the Gauge-Independent Atomic Orbital (GIAO) [85–88] method at the GIAO-PBE0/BS6//PBE0/BS1 level of theory. BS6 is described as the LANL08(f) [46,89] basis sets and corresponding ECP for Cr and Mo, LANL08(d) [48,89] with LANL2DZ ECP for Si, and the IGLO-II basis sets for H, C, and O [90]. The gas-phase computed chemical shift is represented by the difference between the absolute isotropic shielding constant for the reference atom (as computed in TMS) and the absolute isotropic shielding constant for the considered atom within the complex.

Simulated ^{1}H-NMR and ^{13}C-NMR spectra were obtained using an in-house Fortran program by convoluting the computed absolute isotropic shielding values and relative chemical shift with a Gaussian line shape and broadening of 0.025 ppm [91]. To account for peak averaging, the relative isotropic shielding values for chemically equivalent protons and carbons were considered (e.g., the relative isotropic shielding values for the three protons on a methyl group were considered, and the resulting peak was given at the mean chemical shift of these three peaks). To account for temperature-based peak averaging, the chemical shifts of protons and carbons that become chemically equivalent through fluxional processes at each temperature regime were averaged, thereby resulting in coalesced peaks.

Solvation effects on the fluxional processes have been considered by the using the SMD (chloroform) implicit solvation model via self-consistent reaction field (SCRF). Single-point solvation energy computations were performed on gas-phase optimized structures at the SMD-PBE0//PBE0/BS1 level of theory [92].

5. Conclusions

Density functional theory (DFT) was applied to investigate the fluxional processes in $(COT)Cr(CO)_3$ and $(TMCOT)M(CO)_3$ (M = Cr, Mo, and W). ccCA-TM energetics demonstrated that **TS-2** (1,3-shift) is the lowest-energy fluxional process of $(COT)Cr(CO)_3$ ($\Delta E_e^{\ddagger}$ = 17.2 kcal mol^{-1}). It was also discovered that the 1,2-shift represented by **TS-B** (also known as 1,2-shift-a) is the lowest-energy fluxional process for all three $(TMCOT)M(CO)_3$ complexes ($\Delta G^{\ddagger}$ = 12.6 kcal mol^{-1}, 12.8 kcal mol^{-1}, and 13.2 kcal mol^{-1} for M = Cr, Mo, and W, respectively), which was reaffirmed by the analysis of the experimental and computed ^{1}H and ^{13}C-NMR chemical shifts. The computed free energy of activation for **TS-B** of each

of these complexes is consistently slightly lower than the reported experimental results. Implicit solvation slightly alters the relative energies and ordering for the fluxional transition states of all (TMCOT)M(CO)$_3$ complexes. By increasing the temperature to the 112 °C, coalescence of the vinyl hydrogen and methyl peaks, respectively, is observed in the ^{1}H-NMR spectrum of (TMCOT)Cr(CO)$_3$. Similarly, methyl, olefin, and carbonyl carbon peaks coalesce in the high temperature region of the ^{13}C-NMR spectrum of (TMCOT)Cr(CO)$_3$.

Supplementary Materials: The following are available online, Table S1: Computed bond lengths from Cr to COT C atoms (in Å), Table S2: $\Delta G / \Delta G^\ddagger$ values for fluxional transition states of (COT)Cr(CO)$_3$ (in kcal mol^{-1}), Table S3: $\Delta E_e / \Delta E_e^\ddagger$ values for fluxional transition states of (COT)Cr(CO)$_3$ (in kcal mol^{-1}), Table S4: Raw Energies Utilized in Assessment of ccCA-TM Energies Using P Extrapolation (in a.u.), Table S5: $\Delta\Delta E_e / \Delta\Delta E_e^\ddagger$ values for fluxional transition states of (COT)Cr(CO)$_3$ and statistical parameters (R^2 = least squared regression, m = slope, b = y-intercept) in kcal mol^{-1} (relative to ccCA-TM), Figure S1: Plot of $\Delta E_{e,\text{DFT}}$ vs. $\Delta E_{e,\text{ccCA-TM}}$ (in kcal mol^{-1}) for (COT)Cr(CO)$_3$ computed at each level of theory. Table S6: Experimental and computed bond lengths and angles for (TMCOT)Cr(CO)$_3$; computed bond lengths and angles for (TMCOT)Mo(CO)$_3$ and (TMCOT)W(CO)$_3$ (PBE0/BS1 level of theory). (M = Cr, Mo, W), Figure S2: Top-down view of the reported crystal structure of (TMCOT)Cr(CO)$_3$ with atom labels. Hydrogens omitted for clarity, Figure S3: 2D and 3D representation of **TS-G**, Figure S4: 2D and 3D representation of **TS-6** and **2**. Table S7: $\Delta G^\ddagger_{\text{solution}}$ of (TMCOT)M(CO)$_3$ complexes with implicit chloroform solvation model at the SMD-PBE0//PBE0/BS1 level of theory (gas phase $\Delta G^\ddagger$ in parentheses). All relative free energies reported in kcal mol^{-1}. Figure S5: Simulated (colored) gas-phase and experimental (black) ^{1}H-NMR for the lowest energy structure of (TMCOT)Mo(CO)$_3$ at the GIAO-PBEPBE/BS6//PBEPBE/BS1 level of theory. Results given for low-temperature limit (**A**, −10° C), low temperature (**B**, 40 °C), and high-temperature limit (**C**, >80 °C). Experimental ^{1}H-NMR for high temperature limit not reported due to thermal decomposition of (TMCOT)Mo(CO)$_3$ above 80° C. Experimental spectra adapted in part with permission from Cotton, F. A.; Faller, J. W.; Musco, A. Stereochemically Nonrigid Organometallic Compounds. II. 1,3,5,7-Tetramethylcyclo-Octatetraenemolybdenum Tricarbonyl. *J. Am. Chem. Soc.* **1966**, *88* (19), 4506–4507. Copyright (1966) American Chemical Society. Figure S6: Simulated gas-phase (colored, GIAO-PBEPBE/BS6//PBEPBE/auto/BS1) and experimental ^{1}H-NMR for (TMCOT)Cr(CO)$_3$ in three temperature regimes (**A–C**) with corresponding fluxional processes. (CO)$_3$ omitted for clarity. All chemical shifts are relative to tetramethylsilane (TMS). Experimental spectra adapted in part with permission from Cotton, F. A.; Faller, J. W.; Musco, A. Stereochemically nonrigid organometallic molecules. XII. Temperature dependence of the proton nuclear magnetic resonance spectra of the 1,3,5,7-tetramethylcyclooctatetraene tricarbonyl compounds of chromium, molybdenum, and tungsten *J. Am. Chem. Soc.*, **1968**, *90* (6), 1438–1444. Copyright (1968) American Chemical Society. Table S8: Experimental and computed ^{1}H-NMR chemical shifts in (TMCOT)Cr(CO)$_3$ and (TMCOT)Mo(CO)$_3$ at the GIAO-PBEPBE/BS6//PBEPBE/auto/BS1 level of theory (measured in ppm; relative to TMS). Figure S7: 2D-representation of (TMCOT)M(CO)$_3$ (M = Cr, Mo) with hydrogens labeled. (CO)$_3$ omitted for clarity. Table S9: Computed chemical shifts for ^{13}C-NMR in (TMCOT)Cr(CO)$_3$ at the GIAO-PBEPBE/BS6//PBEPBE/auto/BS1 (relative to TMS). See Figure S2 for appropriate atom labeling. Table S10: Basis Sets Used in Study, Molecular Coordinates for (COT)Cr(CO)$_3$ (Å), Molecular Coordinates for (TMCOT)Cr(CO)$_3$ (Å), Molecular Coordinates for (TMCOT)Mo(CO)$_3$ (Å), and Molecular Coordinates for (TMCOT)W(CO)$_3$ (Å).

References

1. Cotton, F.A. Fluxional Organometallic Molecules. *Acc. Chem. Res.* **1968**, *1*, 257–265. [CrossRef]
2. Jutzi, P. Fluxional η[1]-Cyclopentadienyl Compounds of Main-Group Elements. *Chem. Rev.* **1986**, *86*, 983–996. [CrossRef]
3. Jutzi, P.; Burford, N. Structurally Diverse π-Cyclopentadienyl Complexes of the Main Group Elements. *Chem. Rev.* **1999**, *99*, 969–990. [CrossRef] [PubMed]
4. Ma, G.; Deng, J.; Sibi, M.P. Fluxionally Chiral DMAP Catalysts: Kinetic Resolution of Axially Chiral Biaryl Compounds. *Angew. Chem. Int. Ed.* **2014**, *53*, 11818–11821. [CrossRef] [PubMed]
5. Sibi, M.P.; Manyem, S.; Palencia, H. Fluxional Additives: A Second Generation Control in Enantioselective Catalysis. *J. Am. Chem. Soc.* **2006**, *128*, 13660–13661. [CrossRef] [PubMed]
6. Warren, S.; Chow, A.; Fraenkel, G.; RajanBabu, T.V. Axial Chirality in 1,4-Disubstituted (ZZ)-1,3-Dienes. Surprisingly Low Energies of Activation for the Enantiomerization in Synthetically Useful Fluxional Molecules. *J. Am. Chem. Soc.* **2003**, *125*, 15402–15410. [CrossRef] [PubMed]
7. Davies, D.L.; Fawcett, J.; Garratt, S.A.; Russell, D.R. Cp*rhodium and Iridium Complexes with Bisoxazolines: Synthesis, Fluxionality and Applications as Asymmetric Catalysts for Diels–Alder Reactions. *J. Organomet. Chem.* **2002**, *662*, 43–50. [CrossRef]
8. Carmona, D.; Vega, C.; García, N.; Lahoz, F.J.; Elipe, S.; Oro, L.A.; Lamata, M.P.; Viguri, F.; Borao, R. Chiral Phosphinooxazoline-Ruthenium(II) and -Osmium(II) Complexes as Catalysts in Diels−Alder Reactions. *Organometallics* **2006**, *25*, 1592–1606. [CrossRef]
9. Alezra, V.; Bernardinelli, G.; Corminboeuf, C.; Frey, U.; Kündig, E.P.; Merbach, A.E.; Saudan, C.M.; Viton, F.; Weber, J. [CpRu((R)-Binop-F)(H2O)][SbF6], a New Fluxional Chiral Lewis Acid Catalyst: Synthesis, Dynamic NMR, Asymmetric Catalysis, and Theoretical Studies. *J. Am. Chem. Soc.* **2004**, *126*, 4843–4853. [CrossRef] [PubMed]
10. Maji, R.; Ugale, H.; Wheeler, S.E. Understanding the Reactivity and Selectivity of Fluxional Chiral DMAP-Catalyzed Kinetic Resolutions of Axially Chiral Biaryls. *Chem. A Eur. J.* **2019**, *25*, 4452–4459. [CrossRef]
11. Nikitin, K.; O'Gara, R. Mechanisms and Beyond: Elucidation of Fluxional Dynamics by Exchange NMR Spectroscopy. *Chem. A Eur. J.* **2019**, *25*, 4551–4589. [CrossRef] [PubMed]
12. Alshammari, N.; Platts, J.A. Theoretical Study of Copper Binding to GHK Peptide. *Comput. Biol. Chem.* **2020**, *86*, 107265. [CrossRef] [PubMed]
13. Ariafard, A.; Tabatabaie, E.S.; Yates, B.F. Mechanistic Studies of Ligand Fluxionality in [M(H5-Cp)(H1-Cp)(L)2]N. *J. Phys. Chem. A* **2009**, *113*, 2982–2989. [CrossRef]
14. Kirillov, E.; Kahlal, S.; Roisnel, T.; Georgelin, T.; Saillard, J.-Y.; Carpentier, J.-F. Haptotropic Rearrangements in Sandwich (Fluorenyl)(Cyclopentadienyl) Iron and Ruthenium Complexes. *Organometallics* **2008**, *27*, 387–393. [CrossRef]
15. Romão, C.C.; Veiros, L.F. Haptotropic Shifts and Fluxionality of Cyclopentadienyl in Mixed-Hapticity Complexes: A DFT Mechanistic Study. *Organometallics* **2007**, *26*, 1777–1781. [CrossRef]
16. Payard, P.-A.; Perego, L.A.; Grimaud, L.; Ciofini, I. A DFT Protocol for the Prediction of 31P NMR Chemical Shifts of Phosphine Ligands in First-Row Transition-Metal Complexes. *Organometallics* **2020**, *39*, 3121–3130. [CrossRef]
17. Latypov, S.K.; Kondrashova, S.A.; Polyancev, F.M.; Sinyashin, O.G. Quantum Chemical Calculations of 31P NMR Chemical Shifts in Nickel Complexes: Scope and Limitations. *Organometallics* **2020**, *39*, 1413–1422. [CrossRef]
18. Letterman, R.G.; DeYonker, N.J.; Burkey, T.J.; Webster, C.E. Calibrating Reaction Enthalpies: Use of Density Functional Theory and the correlation consistent Composite Approach in the Design of Photochromic Materials. *J. Phys. Chem. A* **2016**, *120*, 9982–9997. [CrossRef] [PubMed]
19. DeYonker, N.J.; Williams, T.G.; Imel, A.E.; Cundari, T.R.; Wilson, A.K. Accurate Thermochemistry for Transition Metal Complexes from First-Principles Calculations. *J. Chem. Phys.* **2009**, *131*, 24106. [CrossRef] [PubMed]
20. Jiang, W.; DeYonker, N.J.; Determan, J.J.; Wilson, A.K. Toward Accurate Theoretical Thermochemistry of First Row Transition Metal Complexes. *J. Phys. Chem. A* **2012**, *116*, 870–885. [CrossRef]
21. Determan, J.J.; Poole, K.; Scalmani, G.; Frisch, M.J.; Janesko, B.G.; Wilson, A.K. Comparative Study of Nonhybrid Density Functional Approximations for the Prediction of 3d Transition Metal Thermochemistry. *J. Chem. Theory Comput.* **2017**, *13*, 4907–4913. [CrossRef] [PubMed]
22. Jiang, W.; Laury, M.L.; Powell, M.; Wilson, A.K. Comparative Study of Single and Double Hybrid Density Functionals for the Prediction of 3d Transition Metal Thermochemistry. *J. Chem. Theory Comput.* **2012**, *8*, 4102–4111. [CrossRef] [PubMed]
23. DeYonker, N.J.; Cundari, T.R.; Wilson, A.K. The correlation consistent Composite Approach (ccCA): An Alternative to the Gaussian-n Methods. *J. Chem. Phys.* **2006**, *124*, 114104. [CrossRef] [PubMed]
24. DeYonker, N.J.; Peterson, K.A.; Steyl, G.; Wilson, A.K.; Cundari, T.R. Quantitative Computational Thermochemistry of Transition Metal Species. *J. Phys. Chem. A* **2007**, *111*, 11269–11277. [CrossRef]

25. DeYonker, N.J.; Grimes, T.; Yockel, S.; Dinescu, A.; Mintz, B.; Cundari, T.R.; Wilson, A.K. The correlation-consistent Composite Approach: Application to the G3/99 Test Set. *J. Chem. Phys.* **2006**, *125*, 104111. [CrossRef]

26. Cotton, F.A.; Hunter, D.L.; LaHuerta, P. Carbon-13 Nuclear Magnetic Resonance Study of the Fluxional Behavior of Cyclooctatetraenetricarbonylchromium, -Molybdenum, and -Tungsten. Tetramethylcyclooctatetraenetricarbonylchromium. *J. Am. Chem. Soc.* **1974**, *96*, 7926–7930. [CrossRef]

27. Bennett, M.J.; Cotton, F.A.; Davison, A.; Faller, J.W.; Lippard, S.J.; Morehouse, S.M. Stereochemically Nonrigid Organometallic Compounds. I. π-Cyclopentadienyliron Dicarbonyl σ-Cyclopentadiene1. *J. Am. Chem. Soc.* **1966**, *88*, 4371–4376. [CrossRef]

28. Cotton, F.A.; Faller, J.W.; Musco, A. Stereochemically Nonrigid Organometallic Compounds. II. 1,3,5,7-Tetramethylcyclo-Octatetraenemolybdenum Tricarbonyl. *J. Am. Chem. Soc.* **1966**, *88*, 4506–4507. [CrossRef]

29. Bennett, M.J.; Cotton, F.A.; Takats, J. Stereochemically Nonrigid Organometallic Molecules. XI. Molecular Structure of (1,3,5,7-Tetramethylcyclooctatetraene)Chromium Tricarbonyl. *J. Am. Chem. Soc.* **1968**, *90*, 903–909. [CrossRef]

30. Cotton, F.A.; Faller, J.W.; Musco, A. Stereochemically Nonrigid Organometallic Molecules. XII. Temperature Dependence of the Proton Nuclear Magnetic Resonance Spectra of the 1,3,5,7-Tetramethylcyclooctatetraene Tricarbonyl Compounds of Chromium, Molybdenum, and Tungsten. *J. Am. Chem. Soc.* **1968**, *90*, 1438–1444. [CrossRef]

31. Whitesides, T.H.; Budnik, R.A. Synthesis and Fluxional Behavior of (.Eta.5-Cycloheptatrienyl)Tricarbonylmanganese. Rearrangement by 1,2 Shifts. *Inorg. Chem.* **1976**, *15*, 874–879. [CrossRef]

32. Gibson, J.A.; Mann, B.E. A reinvestigation of the fluxionality of tricarbonyl(η6-cyclo-octa-tetraene)-chromium and -tungsten using the carbon-13 Forsén-Hoffman spin-saturation method. *J. Chem. Soc. Dalt. Trans.* **1979**, 1021–1026. [CrossRef]

33. Abel, E.W.; Orrell, K.G.; Qureshi, K.B.; Šik, V.; Stephenson, D. H6-Cyclooctatetraene-Metal Complexes Revisited: A Study of Two-Dimensional NMR Exchange Spectroscopy of Tricarbonyl(H6-Cyclooctatetraene)-Chromium and -Tungsten. *J. Organomet. Chem.* **1988**, *353*, 337–342. [CrossRef]

34. Lawless, M.S.; Marynick, D.S. Potential Energy Surfaces for Ring-Rearrangement Processes in Tricarbonyl(Cyclooctatetraene)Chromium(0). *J. Am. Chem. Soc.* **1991**, *113*, 7513–7521. [CrossRef]

35. Frisch, M.J.; Trucks, G.W.; Schlegel, H.B.; Scuseria, G.E.; Robb, M.A.; Cheeseman, J.R.; Scalmani, G.; Barone, V.; Mennucci, B.; Petersson, G.A.; et al. *Gaussian 09, Revision, D.01*; Gaussian, Inc.: Wallingford, CT, USA, 2009; Available online: http://gaussian.com/ (accessed on 25 March 2021).

36. Perdew, J.P.; Burke, K.; Ernzerhof, M. Generalized gradient approximation made simple. *Phys. Rev. Lett.* **1996**, *77*, 3865–3868. [CrossRef] [PubMed]

37. Perdew, J.P.; Burke, K.; Ernzerhof, M. Generalized Gradient Approximation Made Simple. *Phys. Rev. Lett.* **1997**, *78*, 1396. [CrossRef]

38. Parr, R.G.; Yang, W. *Density Functional Theory of Atoms and Molecules*; Oxford University Press: New York, NY, USA, 1989.

39. Adamo, C.; Barone, V. Toward Reliable Density Functional Methods without Adjustable Parameters: The PBE0 Model. *J. Chem. Phys.* **1999**, *110*, 6158–6170. [CrossRef]

40. Becke, A.D. Density-functional Thermochemistry. III. The Role of Exact Exchange. *J. Chem. Phys.* **1993**, *98*, 5648. [CrossRef]

41. Lee, C.; Yang, W.; Parr, R.G. Development of the Colle-Salvetti Correlation-Energy Formula into a Functional of the Electron Density. *Phys. Rev. B* **1988**, *37*, 785–789. [CrossRef]

42. Hamprecht, F.A.; Cohen, A.J.; Tozer, D.J.; Handy, N.C. Development and Assessment of New Exchange-Correlation Functionals. *J. Chem. Phys.* **1998**, *109*, 6264–6271. [CrossRef]

43. Watson, M.A.; Handy, N.C.; Cohen, A.J. Density Functional Calculations, Using Slater Basis Sets, with Exact Exchange. *J. Chem. Phys.* **2003**, *119*, 6475–6481. [CrossRef]

44. Couty, M.; Hall, M.B. Basis Sets for Transition Metals: Optimized Outer p Functions. *J. Comput. Chem.* **1996**, *17*, 1359–1370. [CrossRef]

45. Hay, P.J.; Wadt, W.R. Ab Initio Effective Core Potentials for Molecular Calculations. Potentials for K to Au Including the Outermost Core Orbitals. *J. Chem. Phys.* **1985**, *82*, 299–310. [CrossRef]

46. Hay, P.J.; Wadt, W.R. Ab Initio Effective Core Potentials for Molecular Calculations. Potentials for the Transition Metal Atoms Sc to Hg. *J. Chem. Phys.* **1985**, *82*, 270–283. [CrossRef]

47. Check, C.E.; Faust, T.O.; Bailey, J.M.; Wright, B.J.; Gilbert, T.M.; Sunderlin, L.S. Addition of Polarization and Diffuse Functions to the LANL2DZ Basis Set for P-Block Elements. *J. Phys. Chem. A* **2001**, *105*. [CrossRef]

48. Wadt, W.R.; Hay, P.J. Ab Initio Effective Core Potentials for Molecular Calculations. Potentials for Main Group Elements Na to Bi. *J. Chem. Phys.* **1985**, *82*, 284. [CrossRef]

49. Krishnan, R.; Binkley, J.S.; Seeger, R.; Pople, J.A. Self-Consistent Molecular Orbital Methods. XX. A Basis Set for Correlated Wave Functions. *J. Chem. Phys.* **1980**, *72*, 650–654. [CrossRef]

50. McLean, A.D.; Chandler, G.S. Contracted Gaussian Basis Sets for Molecular Calculations. I. Second Row Atoms, Z=11–18. *J. Chem. Phys.* **1980**, *72*, 5639–5648. [CrossRef]

51. Ehlers, A.W.; Böhme, M.; Dapprich, S.; Gobbi, A.; Höllwarth, A.; Jonas, V.; Köhler, K.F.; Stegmann, R.; Veldkamp, A.; Frenking, G. A Set of F-Polarization Functions for Pseudo-Potential Basis Sets of the Transition Metals Sc-Cu, Y-Ag and La-Au *Chem. Phys. Lett.* **1993**, *208*, 111–114. [CrossRef]

52. Woon, D.E.; Dunning, T.H. Gaussian Basis Sets for Use in Correlated Molecular Calculations. IV. Calculation of Static Electrical Response Properties. *J. Chem. Phys.* **1994**, *100*, 2975–2988. [CrossRef]

53. Woon, D.E.; Dunning, T.H. Gaussian Basis Sets for Use in Correlated Molecular Calculations. V. Core-valence Basis Sets for Boron through Neon. *J. Chem. Phys.* **1995**, *103*, 4572–4585. [CrossRef]

54. Balabanov, N.B.; Peterson, K.A. Systematically Convergent Basis Sets for Transition Metals. I. All-Electron Correlation Consistent Basis Sets for the 3d Elements Sc–Zn. *J. Chem. Phys.* **2005**, *123*, 64107. [CrossRef] [PubMed]

55. Balabanov, N.B.; Peterson, K.A. Basis Set Limit Electronic Excitation Energies, Ionization Potentials, and Electron Affinities for the 3d Transition Metal Atoms: Coupled Cluster and Multireference Methods. *J. Chem. Phys.* **2006**, *125*, 74110. [CrossRef] [PubMed]

56. Kendall, R.A.; Dunning, T.H.; Harrison, R.J. Electron Affinities of the First-row Atoms Revisited. Systematic Basis Sets and Wave Functions. *J. Chem. Phys.* **1992**, *96*, 6796–6806. [CrossRef]

57. Dunning, T.H.; Hay, P.J. *Gaussian Basis Sets for Molecular Calculations*; Springer: Boston, MA, USA, 1977; ISBN 978-1-4757-0889-9.

58. Dolg, M.; Wedig, U.; Stoll, H.; Preuss, H. Energy-adjusted Ab Initio Pseudopotentials for the First Row Transition Elements. *J. Chem. Phys.* **1987**, *86*, 866–872. [CrossRef]

59. Dunlap, B.I.; Connolly, J.W.D.; Sabin, J.R. On Some Approximations in Applications of Xα Theory. *J. Chem. Phys.* **1979**, *71*, 3396–3402. [CrossRef]

60. Dunlap, B.I.; Connolly, J.W.D.; Sabin, J.R. On First-row Diatomic Molecules and Local Density Models. *J. Chem. Phys.* **1979**, *71*, 4993–4999. [CrossRef]

61. Dunlap, B.I. Fitting the Coulomb Potential Variationally in Xα Molecular Calculations. *J. Chem. Phys.* **1983**, *78*, 3140–3142. [CrossRef]

62. Dunlap, B.I. Robust and Variational Fitting: Removing the Four-Center Integrals from Center Stage in Quantum Chemistry. *J. Mol. Struct.* **2000**, *529*, 37–40. [CrossRef]

63. Roothaan, C.C.J. New Developments in Molecular Orbital Theory. *Rev. Mod. Phys.* **1951**, *23*, 69–89. [CrossRef]

64. Wilson, A.; Woon, D.; Peterson, K.; Dunning, T. Gaussian Basis Sets for Use in Correlated Molecular Calculations. IX. The Atoms Gallium Through Krypton. *J. Chem. Phys.* **1999**, *110*, 7667–7676. [CrossRef]

65. Møller, C.; Plesset, M.S. Note on an Approximation Treatment for Many-Electron Systems. *Phys. Rev.* **1934**, *46*, 618–622. [CrossRef]

66. Frisch, M.J.; Head-Gordon, M.; Pople, J.A. A Direct MP2 Gradient Method. *Chem. Phys. Lett.* **1990**, *166*, 275–280. [CrossRef]

67. Frisch, M.J.; Head-Gordon, M.; Pople, J.A. Semi-Direct Algorithms for the MP2 Energy and Gradient. *Chem. Phys. Lett.* **1990**, *166*, 281–289. [CrossRef]

68. Head-Gordon, M.; Pople, J.A.; Frisch, M.J. MP2 Energy Evaluation by Direct Methods. *Chem. Phys. Lett.* **1988**, *153*, 503–506. [CrossRef]

69. Sæbø, S.; Almlöf, J. Avoiding the Integral Storage Bottleneck in LCAO Calculations of Electron Correlation. *Chem. Phys. Lett.* **1989**, *154*, 83–89. [CrossRef]

70. Head-Gordon, M.; Head-Gordon, T. Analytic MP2 Frequencies without Fifth-Order Storage. Theory and Application to Bifurcated Hydrogen Bonds in the Water Hexamer. *Chem. Phys. Lett.* **1994**, *220*, 122–128. [CrossRef]

71. Dunning, T.H. Gaussian Basis Sets for Use in Correlated Molecular Calculations. I. The Atoms Boron through Neon and Hydrogen. *J. Chem. Phys.* **1989**, *90*, 1007–1023. [CrossRef]

72. Čížek, J. On the Use of the Cluster Expansion and the Technique of Diagrams in Calculations of Correlation Effects in Atoms and Molecules. *Adv. Chem. Phys.* **1969**, 35–89. [CrossRef]

73. Purvis, G.D.; Bartlett, R.J. A Full Coupled-cluster Singles and Doubles Model: The Inclusion of Disconnected Triples. *J. Chem. Phys.* **1982**, *76*, 1910–1918. [CrossRef]

74. Scuseria, G.E.; Janssen, C.L.; Schaefer, H.F. An Efficient Reformulation of the Closed-shell Coupled Cluster Single and Double Excitation (CCSD) Equations. *J. Chem. Phys.* **1988**, *89*, 7382–7387. [CrossRef]

75. Scuseria, G.E.; Schaefer, H.F. Is Coupled Cluster Singles and Doubles (CCSD) More Computationally Intensive than Quadratic Configuration Interaction (QCISD)? *J. Chem. Phys.* **1989**, *90*, 3700–3703. [CrossRef]

76. Pople, J.A.; Head-Gordon, M.; Raghavachari, K. Quadratic Configuration Interaction. A General Technique for Determining Electron Correlation Energies. *J. Chem. Phys.* **1987**, *87*, 5968–5975. [CrossRef]

77. Douglas, M.; Kroll, N.M. Quantum Electrodynamical Corrections to the Fine Structure of Helium. *Ann. Phys.* **1974**, *82*, 89–155. [CrossRef]

78. Hess, B.A. Applicability of the No-Pair Equation with Free-Particle Projection Operators to Atomic and Molecular Structure Calculations. *Phys. Rev. A* **1985**, *32*, 756–763. [CrossRef] [PubMed]

79. Hess, B.A. Relativistic Electronic-Structure Calculations Employing a Two-Component No-Pair Formalism with External-Field Projection Operators. *Phys. Rev. A* **1986**, *33*, 3742–3748. [CrossRef] [PubMed]

80. Jansen, G.; Hess, B.A. Revision of the Douglas-Kroll Transformation. *Phys. Rev. A* **1989**, *39*, 6016–6017. [CrossRef]

81. Barysz, M.; Sadlej, A.J. Two-Component Methods of Relativistic Quantum Chemistry: From the Douglas–Kroll Approximation to the Exact Two-Component Formalism. *J. Mol. Struct.* **2001**, *573*, 181–200. [CrossRef]

82. de Jong, W.A.; Harrison, R.J.; Dixon, D.A. Parallel Douglas–Kroll Energy and Gradients in NWChem: Estimating Scalar Relativistic Effects Using Douglas–Kroll Contracted Basis Sets. *J. Chem. Phys.* **2000**, *114*, 48–53. [CrossRef]

83. Williams, T.G.; Deyonker, N.J.; Wilson, A.K. Hartree-Fock Complete Basis Set Limit Properties for Transition Metal Diatomics. *J. Chem. Phys.* **2008**, *128*. [CrossRef] [PubMed]

84. DeYonker, N.J.; Wilson, B.R.; Pierpont, A.W.; Cundari, T.R.; Wilson, A.K. Towards the Intrinsic Error of the correlation consistent Composite Approach (ccCA). *Mol. Phys.* **2009**, *107*, 1107–1121. [CrossRef]

85. McWeeny, R. Perturbation Theory for the Fock-Dirac Density Matrix. *Phys. Rev.* **1962**, *126*, 1028–1034. [CrossRef]
86. Ditchfield, R. Self-Consistent Perturbation Theory of Diamagnetism. *Mol. Phys.* **1974**, *27*, 789–807. [CrossRef]
87. Wolinski, K.; Hinton, J.F.; Pulay, P. Efficient Implementation of the Gauge-Independent Atomic Orbital Method for NMR Chemical Shift Calculations. *J. Am. Chem. Soc.* **1990**, *112*, 8251–8260. [CrossRef]
88. Cheeseman, J.R.; Trucks, G.W.; Keith, T.A.; Frisch, M.J. A Comparison of Models for Calculating Nuclear Magnetic Resonance Shielding Tensors. *J. Chem. Phys.* **1996**, *104*, 5497–5509. [CrossRef]
89. Roy, L.E.; Hay, P.J.; Martin, R.L. Revised Basis Sets for the LANL Effective Core Potentials. *J. Chem. Theory Comput.* **2008**, *4*, 1029–1031. [CrossRef] [PubMed]
90. Kutzelnigg, W.; Fleischer, U.; Schindler, M. *The IGLO-Method: Ab-Initio Calculation and Interpretation of NMR Chemical Shifts and Magnetic Susceptibilities BT-Deuterium and Shift Calculation*; Fleischer, U., Kutzelnigg, W., Limbach, H.-H., Martin, G.J., Martin, M.L., Schindler, M., Eds.; Springer: Berlin/Heidelberg, Germany, 1991; pp. 165–262.
91. Press, W.H. *Numerical Recipes in FORTRAN: The Art of Scientific Computing*, 2nd ed.; Cambridge University Press: Cambridge, UK, 1992.
92. Marenich, A.V.; Cramer, C.J.; Truhlar, D.G. Universal Solvation Model Based on Solute Electron Density and on a Continuum Model of the Solvent Defined by the Bulk Dielectric Constant and Atomic Surface Tensions. *J. Phys. Chem. B* **2009**, *113*, 6378–6396. [CrossRef] [PubMed]